IEEE Access
Multidisciplinary ⋮ Rapid Review ⋮ Open Access Journal

Received 1 February 2024, accepted 21 February 2024, date of publication 23 February 2024, date of current version 29 February 2024.

Digital Object Identifier 10.1109/ACCESS.2024.3369415

RESEARCH ARTICLE

A Code-Orthogonal PMCW Transmission Scheme for Improving Communications Performance in JCAS Systems

YANPENG SU, (Member, IEEE), VICTOR SHATOV, (Member, IEEE), NORMAN FRANCHI, (Member, IEEE), AND MAXIMILIAN LÜBKE, (Member, IEEE)
Chair of Electrical Smart City Systems, Friedrich-Alexander-Universität Erlangen-Nürnberg, 91058 Erlangen, Germany

Corresponding author: Yanpeng Su (yanpeng.su@fau.de)

This work was supported in part by the Federal Ministry of Education and Research (BMBF) of Germany through the Project KOMSENS-6G under Grant 16KISK126, and in part by German Research Foundation (DFG) under Grant DR 639/18-4.

ABSTRACT Joint communications and sensing (JCAS) is regarded as a major technology building block in 6G networks. The combination of communications and radar sensing systems benefits from saved hardware costs, reduced energy consumption, and less spectrum occupation. Phase-modulated continuous waveform (PMCW) is regarded as an attractive candidate waveform for future automotive JCAS systems due to its perfect anti-interference properties and radar sensing performance. However, PMCW-based JCAS systems usually suffer from extremely low data rates and undesirable communications reliability in dynamic environments, limiting their applicability in traffic scenarios, where the propagation channel may suffer from a high Doppler shift and spread and a large data throughput is expected. To overcome the shortcomings, in this work, a novel PMCW approach with simultaneously transmitted pilot and data sequences, named code-orthogonal PMCW (CO-PMCW), is introduced. The presented CO-PMCW approach benefits from significantly improved data rate and robustness in dynamic environments. Regarding the differences in system architecture between PMCW and CO-PMCW, the authors verified the advantages and investigated the potential side effects of the CO-PMCW system. The properties including the interference between the pilot and data, influence on transmission power, behavior in multipath fading channels, etc. are measured. The result shows that the presented CO-PMCW approach significantly improves the communications performance with slightly influenced radar properties. Based on the simulation result, the application feasibility and scenarios of the CO-PMCW-based JCAS system are analyzed.

INDEX TERMS 77 GHz, channel fading, Doppler effect, integrated sensing and communications (ISAC), joint communications and sensing (JCAS), JCRS, mmWave, physical layer design, PMCW, spread spectrum, V2X.

I. INTRODUCTION

In recent years, the millimeter-wave (mmWave) band (30 GHz - 300 GHz) has become the focus of research on automotive communications and radar systems due to the high throughput and accuracy brought by wide bandwidth [1]. Currently, most vehicular radar systems are operated at the 77 GHz band since it allows a smaller antenna size as well as a wider bandwidth, benefiting from higher sensing resolution and accuracy [2], [3]. At the 77 GHz band, the frequency band from 76-77 GHz is usually used for long-range radar (LRR) systems, while the short-range radar (SRR) and mid-range radar (MRR) systems occupy the band of 77-81 GHz for higher resolution [3], [4]. On the other hand, the vehicular communications systems are also expected to be operated at the 77 GHz band [1], [5]. The so-called vehicle-to-everything (V2X) communications allow vehicles to share information like their movement and road conditions, providing a more comfortable and safer driving experience and reducing traffic congestion [6], [7].

The associate editor coordinating the review of this manuscript and approving it for publication was Minseok Kim.

With the development of information and electronic technologies, the number of vehicles equipped with communications and radar sensing systems has increased rapidly in the last decades. It is foreseeable that this number will grow even faster in the future due to the wide application of advanced driver assistance system (ADAS) and self-driving systems [8]. However, this will inevitably cause harsh channel conditions due to interference, and separated communications and sensing systems lead to more space and hardware costs. To overcome these problems, the method known as JCAS [9], [10], or integrated sensing and communications (ISAC) [11], [12], has been put forward and received high attention in recent years. JCAS enables coordination of radar and communications and aims to allow the communications and radar systems to share the same hardware, spectrum, and even waveform, benefiting from the saved band, reduced costs, and less energy consumption. Therefore, JCAS is seen as one of the major technologies in the future 6G networks [13], [14].

The idea of JCAS is to integrate the communications and radar sensing into one system by allowing radar waveforms to carry data symbols, allowing the radar receiver to extract information from the communications signals, or designing a system jointly with a flexible trade-off between communications and radar sensing, corresponding to three categories: radar-centric design, communications-centric design, and joint design and optimization [15], [16].

There already exist several waveform candidates for JCAS systems design. Currently, frequency-modulated continuous waveform (FMCW) is the most common radar waveform and has been widely used in modern automotive radar systems [17]. The main disadvantages of FMCW are the poor capability to carry data and the sensitivity to interference [17], [18], [19], [20], and the analogy modulation scheme limits the adaptability and flexibility of the system [21]. To this end, digitally-modulated waveforms, like PMCW and orthogonal frequency-division multiplexing (OFDM), are expected to be applied in future JCAS systems. OFDM allows an extremely high data rate transmission and has been widely utilized in modern communications networks. Therefore, OFDM has a high potential to be applied in cellular network-based JCAS systems [16]. However, OFDM-modulated signals have a common problem of high peak-to-average power ratio (PAPR) [22], reducing average transmission power and resulting in shorter propagation distance. Additionally, the maximum tolerable range and velocity of OFDM-based JCAS systems are further limited to avoid inter-symbol interference (ISI) and inter-carrier interference (ICI) [18], [23], which may make OFDM not suitable for automotive applications, where the Doppler effect is usually high and the distance between the vehicles and other objects fastly varies. In contrast, PMCW is a single-carrier waveform and therefore, benefits from low PAPR [24]. The modulation of direct sequence spread spectrum (DSSS) suppresses interference, improving the reliability and applicability in future traffic scenarios [25].

As PMCW is a radar-centric waveform, the communications system is integrated based on the radar system. Therefore, the communications function is inevitably limited. It has been explained in [18] that the communications resource efficiency of the PMCW-based JCAS systems is quite low and usually fixed by the radar configuration and parameters, resulting in a non-flexible communications system. To address these shortcomings, in [26], the authors have introduced a novel PMCW system where the pilot and data sequences are transmitted simultaneously and separated via orthogonal spreading codes, named by code-orthogonal PMCW (CO-PMCW) in this paper, and the conventional PMCW approach is briefly referred to as PMCW. The result showed that the system with CO-PMCW benefits from improved data rates and flexible communications system configuration. Afterward, the performance improvement of the CO-PMCW approach in dynamic environments was analyzed. However, the work in [26] focused on the fundamentals and theoretical analysis of CO-PMCW, whereas its advantages and potential side effects were not verified in the experiment. In this work, the properties of the CO-PMCW approach are investigated. The contributions of this paper can be summarized as follows:

- Describing the physical layer signal processing scheme of the PMCW-based JCAS systems and analyzing its advantages and limitations.
- Introducing the fundamentals of CO-PMCW, analyzing its advantages and potential side effects compared to the conventional one.
- Comparing the performance of PMCW and CO-PMCW, evaluating their differences in PAPR, interference level, behavior in dynamic environments, and the impact of multipath fading on service reliability.
- Discussing the appropriate application scenarios of CO-PMCW and methods to overcome its shortcomings.

This paper is structured as follows: In section II, the fundamentals, system architecture, as well as the shortcomings of the PMCW-based JCAS systems are described. Then addressing the shortcomings, the CO-PMCW approach with simultaneously transmitted pilot and data is introduced in section III. Its improvement in communications performance and potential side effects are explained in section IV. Section V lists and compares the parameters of the PMCW and CO-PMCW systems, then the simulation environment and channel parameters are introduced. Afterward, in section VI, the authors analyzed the pros and cons of the CO-PMCW approach and verified the assumptions in the simulation. At last, in section VII, the benefits and shortcomings of CO-PMCW are summarized, and its limitations are explained. In response to the properties, its suitable application scenarios are discussed.

II. CONVENTIONAL PMCW APPROACH

This section briefly reviews a JCAS system structure based on the conventional PMCW approach. This work focuses on single-input single-output (SISO) systems to evaluate the

performance of the PMCW- and CO-PMCW-based systems. The signal processing scheme and parameters of the SISO systems are detailed described. The multiple-input multiple-output (MIMO) JCAS systems extract information like angle of arrival (AoA) besides range and velocity and have been widely discussed in other literature like [27] and [28]. Since angular estimation is mainly related to antenna design instead of waveform design, the MIMO system is not included in this work whereas the advantages and shortcomings of PMCW are analyzed at the end of this section.

The PMCW system structure has been proposed and introduced in previous literature like [25], [29], [30], [31], and [32]. Fig. 1 illustrates the corresponding signal transmission and processing scheme. The PMCW transmitter transmits the pilot and data symbols sequentially in each transmission period, where one pilot symbol is usually followed by several data symbols, whose number is denoted by $C-1$. After combining the pilot and data symbols, the signal is spread by pseudo-random noise sequence (PRNS), whose length is denoted by L_c. Afterward, the pilot and data symbols are usually repeated A times to have a higher processing gain. Therefore, each transmission period includes an A-times repeated pilot symbols and $C-1$ A-times repeated data symbols. Considering the duration of each symbol is $A \cdot L_c \cdot T_c$, where T_c denotes the chip period, each transmission period takes a time length of $C \cdot A \cdot L_c \cdot T_c$. Therefore, the data rate with the modulation scheme of binary phase-shift keying (BPSK) is

$$R_{\mathrm{T,PMCW}} = \frac{C-1}{C \cdot A \cdot L_c \cdot T_c}, \tag{1}$$

the corresponding spectrum efficiency Γ_{PMCW} and data spreading gain G_{PMCW} are given by

$$\Gamma_{\mathrm{PMCW}} = \frac{R_{\mathrm{T,PMCW}}}{B} = \frac{C-1}{2 \cdot C \cdot A \cdot L_c}, \tag{2}$$

$$G_{\mathrm{PMCW}} = A \cdot L_c, \tag{3}$$

whereby the data rate and spectrum efficiency of the communications part are limited to a very low level, while the data processing gain is fixed at a high level. Therefore, the communications functions are limited and non-flexible, which cannot meet the requirement of high spectrum efficiency and resilient functions at the age of 6G [12], [13], [33].

The modulated digital signal is converted to analog by a digital-to-analog converter (DAC), modulated to 77 GHz by the radio frequency (RF) up-converter, and then transmitted by the antenna. At the communications receiver, the received signal $r(t)$ is moved back to the baseband and then converted to a digital signal with a sampling period of T_c. The S/P converter collects L_c consecutive samples and transforms them into a 1-D array. As PMCW has a similar signal modulation scheme as CDMA, the communications system uses a Rake receiver to estimate the multipath fading channel [34]. In this work, for simplification, least square (LS) is chosen as the channel estimation method, and linear interpolation is used to compensate for the phase shift between the two pilot symbols caused by the Doppler effect. The interpolation method has been widely used in channel estimation and benefits from fewer pilot symbols insertion [35], [36]. After channel estimation, the communications receiver implements channel equalization or maximum ratio combining (MRC) and data detection in turns of data [37].

At the radar receiver, the analog part is the same as the communications receiver. The S/P converter collects L_c samples and transforms the samples into a 1-D array. The array is then processed by a correlator bank with a size of L_c, an accumulator with a factor of A, and an FFT estimator with a length of N. Note A could neither be too small since the processing gain is also reduced nor be too large because too long accumulation period suffers from significant phase rotations due to the Doppler effect. As a result, the radar receiver outputs a range-Doppler map, where the delay and Doppler information are indicated in the fast time domain and slow time domain, respectively. The total radar processing gain is therefore given by

$$G_r = 10\log_{10}(L_c A N). \tag{4}$$

III. PRESENTED CO-PMCW APPROACH

To overcome the shortcomings of PMCW, in [26], the authors have presented a novel approach with simultaneously and continuously transmitted pilot and data. To the best of the author's knowledge, there is no other research that can significantly improve the communications function of PMCW up to now. The CO-PMCW-based JCAS system architecture as well as its benefits and potential side effects are described in this section.

A. TRANSMITTER

The system architecture is illustrated in Fig. 2. Different from the general PMCW approach, the pilot and data are simultaneously transmitted and spread by different PRNSs, noted by $\mathrm{PRNS_p}$ and $\mathrm{PRNS_d}$, respectively. The computational effort or hardware structure of the transmitter is slightly increased as it needs to generate two PRNSs simultaneously. The cross-correlation function (CCF) and the sidelobes of autocorrelation function (ACF) of the PRNSs are desired to be as low as possible to guarantee strong isolation between the pilot and data and a high peak to sidelobe ratio (PSLR) at the output of correlator bank [38]. In this work, Gold codes are chosen as PRNSs due to their large set size and relatively good ACF and CCF [39].

Afterward, the pilot is phase-shifted by 90° to have better isolation from the data sequence and reduce the PAPR, which is 1 and 2 for BPSK-modulated PMCW signals with and without the phase shift, respectively. Nevertheless, the PAPR may become higher with modulation schemes like quadrature phase shift keying (QPSK) and quadrature amplitude modulation (QAM), which is seen as a side effect. Details are explained in section IV-A.

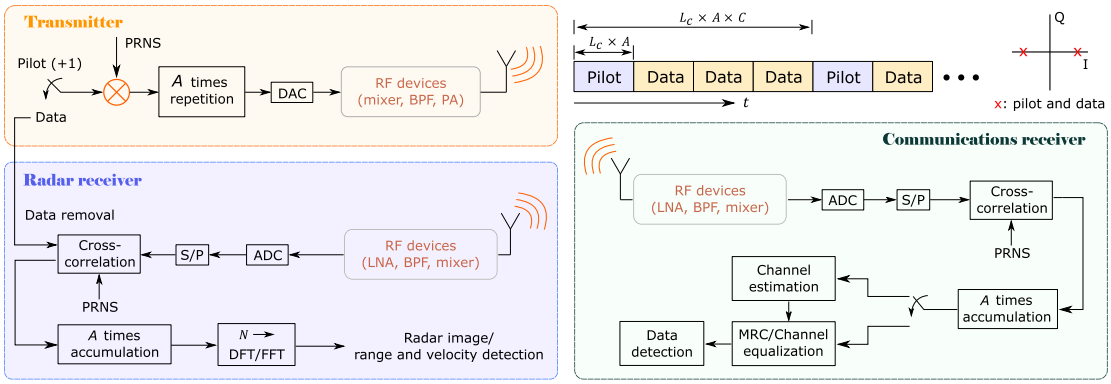

FIGURE 1. PMCW-based SISO JCAS system structure. The pilot and data symbols are transmitted sequentially, each symbol has the same duration according to radar parameters configuration.

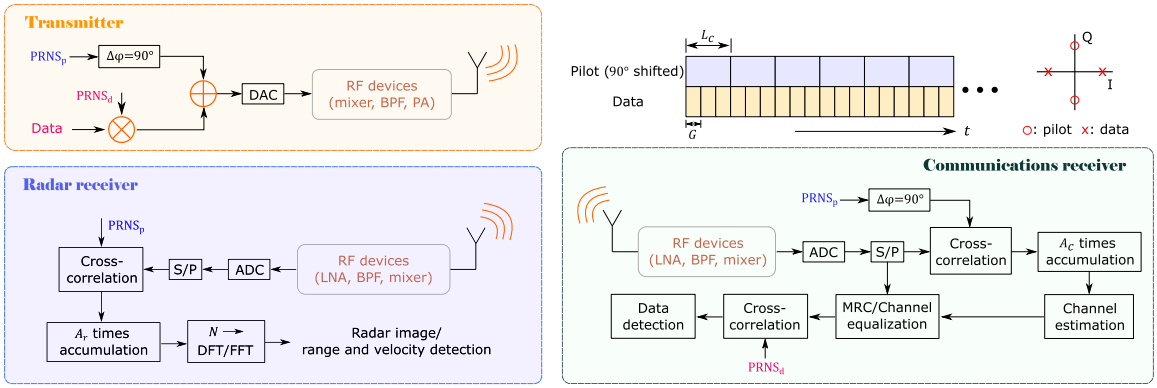

FIGURE 2. CO-PMCW-based SISO JCAS system structure. The pilot and data symbols are transmitted simultaneously and continuously. They are separated by two almost orthogonal PRNSs and a phase shift of 90°. The communications system is completely independent of radar functions, thus the data rate is flexibly choosable. The continuously transmitted pilot enables the communications receiver to perform an uninterrupted channel estimation, improving system performance in dynamic environments.

Since the radar receiver only utilizes the pilot for sensing estimation, there is no relationship between the data sequence and the radar receiver, the data rate is liberated from radar functions, enabling a higher data rate and flexible data signal parameterization. The data spreading gain and spectrum efficiency are given by

$$G_{\mathrm{CO}} = \frac{R_{\mathrm{T,CO}}}{R_{\mathrm{c}}} = \frac{T_{\mathrm{c}}}{T_{\mathrm{D,CO}}}, \tag{5}$$

$$\Gamma_{\mathrm{CO}} = \frac{R_{\mathrm{T,CO}}}{B} = \frac{1}{2G_{\mathrm{CO}}}, \tag{6}$$

where R_{c} and $T_{\mathrm{D,CO}}$ denote the chip rate and data period of the CO-PMCW approach. Note G_{CO} is freely choosable, and could also be lower than L_{c}, leading to a higher data rate but worse anti-interference performance due to non-periodical correlation.

The flexible data rate provides a trade-off between the Doppler effect and signal-to-noise ratio (SNR). On the one hand, higher spreading gain benefits from higher energy per bit to noise power spectral density ratio (E_{b}/N_0) and less frequency selectivity; on the other hand, smaller G_{CO} reduces the impact of the Doppler effect since the Doppler effect causes time selectivity, and shorter symbol duration benefits from slower fading process [26]. In summary, the flexible data rate and spreading gain provide a resilient function facing noise and channel dynamics.

The analog system structure remains the same: at the transmitter side, the signal is converted to an analog signal with a carrier frequency of 77 GHz and transmitted by the antenna array. At the receiver side, the received signal or echo is converted back to a baseband digital signal for subsequent processing.

B. COMMUNICATIONS RECEIVER

Different from the PMCW system, channel estimation and data detection are parallel implemented at the communications receiver, thus the computational effort is approximately doubled. The channel estimation system structure is the same as the PMCW system, it uses a Rake receiver to estimate the channel condition and combines the data signals from different paths via MRC. Note not only the data rate but also the accumulation factor A_{c} are independent of the radar function, where the accumulation factor is denoted by A_{r}. In [26], the authors have proved that a flexible A_{c} benefits from resilience to the impact of the Doppler effect and noise level. Additionally, there is a trade-off between E_{b}/N_0 and the data rate. Fig. 3 shows an example of the trade-off, where the blue rectangular- and red diamond-marked curves

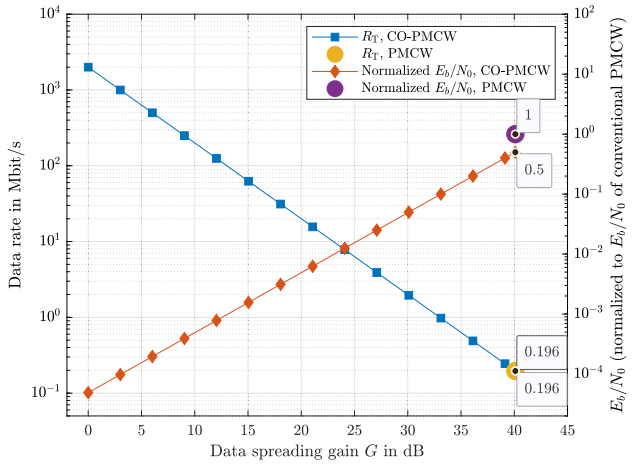

FIGURE 3. Data rate versus E_b/N_0 curve. E_b/N_0 is normalized to the value of PMCW. The data rate of the CO-PMCW-based system is inversely proportional to E_b/N_0, while the parameters of the PMCW approach are fixed. The flexible G results in a resilience function to noise and quality of service (data rate).

denote the data rate and normalized E_b/N_0 of CO-PMCW versus data spreading gain curves. The values are calculated according to the system parameters given in Table 2. The data rate and normalized E_b/N_0 of PMCW are represented by yellow and purple points, respectively. The data rate of the CO-PMCW approach decreases with the growing data spreading gain, while E_b/N_0 increases. When $G_{CO} = G_{PMCW}$, the data rates of the two systems are the same, but the E_b/N_0 with the CO-PMCW approach is half that of the PMCW system since the pilot is transmitted at the same time. Note that G of CO-PMCW can be further increased and exceed the spreading gain of the PMCW approach, resulting in a higher E_b/N_0 and, however, lower data rate.

Benefiting from the continuously transmitted pilot symbols, the channel estimator can track the channel condition without interruption, improving transmission reliability in dynamic environments. In the data detection process, after being despread by $PRNS_d$, the data symbols are combined, demodulated, and detected. One problem is that there exists interference between $PRNS_p$ and $PRNS_d$, which is a potential side effect of CO-PMCW.

C. RADAR RECEIVER

The structure and computation amount of the radar receiver is not influenced by applying the new approach. It still includes a correlator bank for range estimation, an accumulator for higher processing gain, and an FFT calculator for velocity estimation. Note that only the pilot sequence $PRNS_p$ is utilized for radar sensing, whose accumulation time A_r is different from A_c at the communications receiver. The radar receiver outputs a range-Doppler map, where the range and velocity information are indicated in the fast time domain and slow time domain, respectively. Similar to the communications system, the radar performance also suffers from interference caused by simultaneous transmission, which will be investigated in section VI-A.

TABLE 1. Maximum and minimum power of data symbols different modulation schemes with Gray mapping. The average power is normalized to 1 W.

	P_{max} in W	P_{min} in W
BPSK	1	1
QPSK	1	1
8-PSK	1	1
16-QAM	1.8	0.2
32-QAM	1.7	0.1
64-QAM	2.33	0.0476
128-QAM	2.07	0.0244
256-QAM	2.65	0.0118
512-QAM	2.28	0.0061
1024-QAM	2.82	0.0029

IV. RELEVANT PARAMETERS AND THEORETICAL PERFORMANCE ANALYSIS

In this part, the PAPR and signal power issues are analyzed. Then the radar and communications functions of the PMCW and CO-PMCW systems are analyzed and compared theoretically. The advantages of the CO-PMCW system in dynamic environments as well as the limitations in achievable data rate are highlighted.

A. PEAK TO AVERAGE POWER RATIO AND SIGNAL POWER ISSUES

PAPR is a factor that limits the transmission power. To avoid distortion, the RF components are desired to operate in the linear region [40]. Waveforms like OFDM usually suffer from a high PAPR, therefore, reducing the average transmission power. Low PAPR could be regarded as an advantage of PMCW. However, the PAPR increases with higher modulation schemes like QAM. The CO-PMCW system performs a simultaneous transmission of the pilot and data, where the pilot is PRNS with values of $\pm j$ after the phase shift, and the data symbols are modulated by BPSK, QPSK, M-QAM, etc. This, on the one hand, leads to different self-interference (SI) with different symbols and, on the other hand, increases the PAPR.

The power difference between symbols grows with M, see Table 1, where the average power P_{avg} is normalized to 1 W. To avoid unfeasible transmission of the symbols with low power and ensure a reliable channel estimation, the power of the pilot sequence can neither be too high as the data symbols with low power may hide below the interference from the pilot, nor be too low as the pilot may become undetectable due to the interference from data. In this work, the average power of the modulated data sequence is set to the power of the pilot sequence. The modulated data symbols are phase-shifted by 45° so that the minimum angle between the symbols and the y-axis (i.e., the pilot) is maximized, minimizing the PAPR. Fig. 4 shows an example of the signal constellation with QPSK-modulated data symbols, where the blue point, red cross, and yellow asterisk denote the constellation of the pilot, QPSK-modulated data, and the combined signal.

Fig. 5 shows the signal PAPR of the PMCW (blue line) and CO-PMCW (red line) approaches for different modulation schemes. Not only M, the parallel transmission scheme also

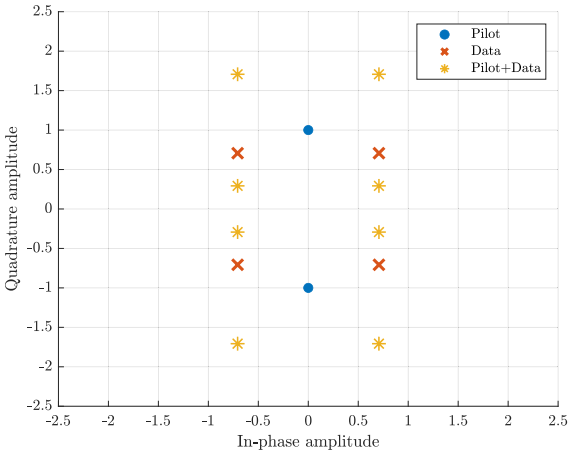

FIGURE 4. Signal constellation with modulation of QPSK.

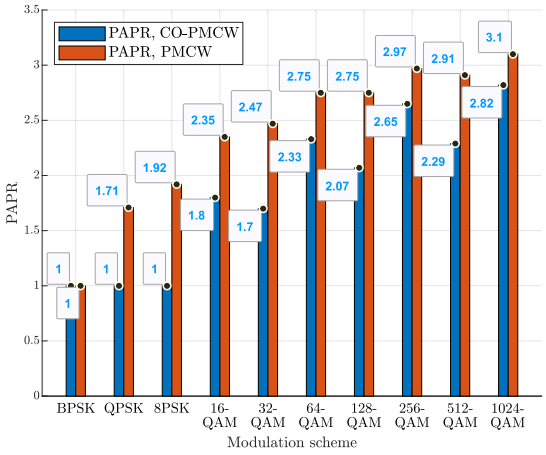

FIGURE 5. PAPR of PMCW- and CO-PMCW-based JCAS systems. The PAPR is increased by the simultaneous pilot and data transmission, further limiting the transmission power.

increases the PAPR. To avoid distortion produced by RF hardware nonlinearity, the average transmission power of the CO-PMCW approach should be lower than that of the conventional PMCW approach. In CO-PMCW transmission, the power of the pilot and data sequences is further halved due to the parallel transmission, leading to lower SNR at the receiver side and further limiting the maximum propagation distance, which is a drawback of CO-PMCW.

B. RADAR PARAMETERS

As there is no modification at the radar receiver side, the signal processing parameters and radar parameters of PMCW and CO-PMCW-based systems are the same. For a radar system, the designers are mainly concerned about its processing time, maximum unambiguous range and velocity, resolution or accuracy, and processing gain [21]. The calculation of these parameters has been introduced in literature like [41] and [42], and is shortly summarized in this section.

The dwell time, i.e., the theoretical processing time, is given by

$$T_{\mathrm{d}} = T_{\mathrm{c}} \cdot L_{\mathrm{c}} \cdot A \cdot N. \tag{7}$$

The range information is extracted from the correlator bank. The chip rate and the size of the correlator bank are relevant to the maximum unambiguous range r_{u} and range resolution Δr, which are defined as

$$r_{\mathrm{u}} = \frac{c \cdot L_{\mathrm{c}} \cdot T_{\mathrm{c}}}{2}. \tag{8}$$

$$\Delta r = \frac{c \cdot T_{\mathrm{c}}}{2}. \tag{9}$$

The velocity of the targets is calculated via FFT, whose input sampling rate is relevant to the maximum unambiguous velocity v_{u}, and the length N determines the velocity resolution Δv:

$$v_{\mathrm{u}} = \frac{c}{4 \cdot f_{\mathrm{c}} \cdot A \cdot L_{\mathrm{c}} \cdot T_{\mathrm{c}}}, \tag{10}$$

$$\Delta v = \frac{c}{2 \cdot f_{\mathrm{c}} \cdot N \cdot A \cdot L_{\mathrm{c}} \cdot T_{\mathrm{c}}} = \frac{c}{2 \cdot f_{\mathrm{c}} \cdot T_{\mathrm{d}}}. \tag{11}$$

Note the interference of the data sequence may reduce the PSLR in the range profile on the range-Doppler map as it can be regarded as an interference signal with the same power as the desired one. This may further reduce the maximum detectable range. The impact of this interference is evaluated in section VI-A.

C. COMMUNICATIONS FUNCTION IN FADING CHANNELS

As for the traditional pure communications systems, the designers focus more on resource efficiency (like spectrum efficiency) and compatibility with different channel conditions including delay spread τ_{DS}, Doppler effect f_{D}, coherence bandwidth B_{coh}, and coherence time T_{coh} [43], [44], [45], [46].

From the perspective of resource efficiency and throughput, the performance of PMCW is unattractive as the data rate is determined by the radar functions, leading to a low and inflexible data rate. The only solution by increasing C has a very limited effect and may lead to worse reliability in dynamic environments since the density of the pilot symbols is reduced. Opposite to PMCW, CO-PMCW has an extremely improved data rate. As given in (5), where $G_{\mathrm{CO}} \geq 1$, the highest achievable data rate is the same as the chip rate R_{c}, resulting in higher spectrum efficiency.

However, a high data rate may increase frequency selectivity and lead to higher delay spread at the Rake receiver: on the one hand, when $G_{\mathrm{CO}} < L_{\mathrm{c}}$, the orthogonal autocorrelation property of the PRNS is destroyed. In that case, lower spreading gain results in less suppression of multipath interference, which increases the delay spread in the branches of the Rake receiver, leading to more ISI. On the other hand, the coherence bandwidth of the despread signal is narrowed since the delay spread is increased, while the bandwidth of data symbols is extremely extended and may approach or even exceed the coherence bandwidth, leading to frequency selective fading. Therefore, the system performance with multipath fading deteriorates, which is one of the reasons that realizing an extremely high data rate transmission in a PMCW-/CDMA-based system is difficult. To avoid the

impact of delay spread and frequency selectivity, the data spreading gain should be high enough that the interference of other channel components is sufficiently suppressed.

Different from delay spread, the Doppler effect f_D and channel coherence time T_{coh} limit the lower band of data rate and the time distance between the pilot symbols [35], [47]. For PMCW systems, considering the impact on channel estimation, the transmission period C, i.e., the distance between two pilot symbols, should be sufficiently low:

$$2\pi \cdot f_D \cdot C \cdot A \cdot L_c \cdot T_c \ll \pi, \tag{12}$$

$$C \cdot A \cdot L_c \cdot T_c \ll T_{coh} \propto \frac{1}{f_D}, \tag{13}$$

where (12) and (13) show the limitations considering the influence of the Doppler effect, and the coherence time on channel estimation and interpolation, they illustrate the same problem that the data period and pilot distance are limited by channel dynamics. Since JCAS is expected to be applied in many highly dynamic environments like vehicular information systems and traffic management, a high pilot density is expected, thus the data rate of PMCW systems is further limited.

For CO-PMCW, as the pilot and data sequences are simultaneously transmitted, the impact of channel dynamics on both sequences should be considered. Rewriting (12) and (13), we obtain

$$\begin{cases} 2\pi \cdot f_D \cdot A_c \cdot L_c \cdot T_c \ll \pi \\ 2\pi \cdot f_D \cdot T_{D,CO} \ll \pi \Rightarrow R_{T,CO} \gg 2f_D \end{cases}, \tag{14}$$

and

$$\begin{cases} A_c \cdot L_c \cdot T_c \ll T_{coh} \propto \dfrac{1}{f_D} \\ T_{D,CO} \ll T_{coh} \end{cases}, \tag{15}$$

where the upper and lower branches in (14) and (15) denote the requirements on the pilot accumulation factor and data period, respectively. Note if the channel equalization is implemented before data despreading, the channel parameters are removed before data sequence processing. In this case, the limitation of the data period $T_{D,CO}$ is released.

Compared with PMCW, the requirements are relatively more relaxing since the pilot is continuously transmitted and the accumulation time A_c is flexible, hence the communications reliability in dynamic environments is improved. Summarizing (12)-(15) and considering the relationship between the Doppler effect and relative velocity, the maximum tolerable relative speed of the PMCW- and CO-PMCW-based communications system is given by

$$v_{c,max,PMCW} \ll \frac{c}{2 \cdot C \cdot f_c \cdot A \cdot L_c \cdot T_c}, \tag{16}$$

$$v_{c,max,CO} \ll \frac{c}{2f_c \cdot A_c \cdot L_c \cdot T_c}, \tag{17}$$

where $C \geq 2$ ($C = 1$ denotes the case that no data is transmitted in PMCW systems). The maximum tolerable speed of the CO-PMCW communications function is significantly higher than PMCW. Additionally, A_c and $T_{D,CO}$ are freely choosable, benefiting from a high adaptivity and flexibility in coping with different channel conditions. The performance of the communications systems in different fading channels is investigated in section VI-B and section VI-C.

The CO-PMCW approach realizes almost independent communications and radar functions since the communications and radar systems can configure themselves without any influence on each other. Therefore, the proposed CO-PMCW waveform design is considered as a joint design, instead of a radar-centric design or communications-centric design.

In summary, the analyzed advantages and potential side effects of the CO-PMCW approach are listed here:

- Advantages:
  - High data rate and spectrum efficiency.
  - Joint design: the communications and radar functions are independent of each other.
  - Flexible communications system: resilience to the Doppler effect and SNR; trade-off between frequency and time selectivity.
  - Higher maximum tolerable speed for communications function.
- Potential side effects/limitations:
  - Interference between the pilot and data sequences.
  - Reduced power for both the pilot and data due to simultaneous transmission.
  - Higher PAPR with complex modulation schemes.
  - Still limited data rate due to multipath fading.
  - Increased transmitter and communications receiver complexity or computational effort due to the parallel processing.

This work aims to address the above-discussed properties and evaluate the feasibility of applying CO-PMCW in future traffic scenarios. In section V, the system parameters as well as the simulation environment are introduced. In section VI, the impact of the increased interference and channel conditions is investigated in simulation.

V. SYSTEM CONFIGURATION AND SIMULATION ENVIRONMENTS

In order to have a comprehensive comparison between PMCW and CO-PMCW, the system model and parameters need to be configured. In [26], the authors have built the PMCW systems on Matlab/Simulink, and the system parameters are given in Table 2. The model provides a short-range JCAS system operating at 77 GHz with a bandwidth of 4 GHz, resulting in a chip period T_c of 0.5 ns. The Gold sequences with a length of 1023 are chosen as spreading sequences. The transmission period C of PMCW defaults to five, where a pilot symbol is followed by four data symbols in each transmission period. The accumulation times A, A_c, and A_r default to 10, whereas the pilot accumulation time A_c at the communications receiver of CO-PMCW is freely choosable. The resulting data rates for the PMCW- and CO-PMCW-based systems are 156.4 kbit/s and 50 Mbit/s,

TABLE 2. Overview of the system parameters.

Parameters	PMCW	CO-PMCW
Carrier frequency f_c	77 GHz	
Bandwidth B	4 GHz	
Chip period T_c	0.5 ns	
PRNS	Gold codes with length of $L_c = 1023$	
Modulation scheme	BPSK	
Transmission period C	5	-
Accumulation time	$A = 10$	$A_c = 10$ $A_r = 10$
Data rate R_T	156.4 kbit/s	50 Mbit/s
Data spreading gain G	40.1 dB	16 dB
Maximum tolerable relative speed (comm.) $v_{c,max}$	$\ll$ 76.2 m/s	$\ll$ 380.9 m/s
Fast Fourier transform (FFT) size N	2048	
Maximum unambiguous range r_u	76.725 m	
Range resolution Δr	0.075 m	
Maximum unambiguous relative velocity v_u	190.43 m/s	
Velocity resolution Δv	0.186 m/s	
Radar signal processing gain G_r	73.2 dB	

corresponding to data spreading gains of 40.1 dB and 16 dB, respectively. Not only the data rate but also the maximum tolerable relative speed of the communications system is significantly improved by CO-PMCW, without influence on radar parameters like r_u, Δr, v_u, Δv, and signal processing gain G_r.

Not only the system parameters but also the channel conditions are introduced in this section. The channel model has been built on WinProp, a 3D ray-tracing software solution provided by Altair, and introduced in [34] and [41]. In this work, rural and highway scenarios are considered, where two vehicles are driving in the opposite direction, as illustrated in Fig. 6. The left car is chosen as the transceiver which transmits the JCAS signal to the target vehicle and receives the echo for radar sensing, and the right car acts as the communications receiver and detects communications information from the received signal. The obtained channel parameters are listed in Table 3. Note in Table 3, the reflection gain is specified as radar cross section (RCS) with a unit of dB per one square meter (dBsm). RCS is typically 10-20 dBsm for cars. The reflection gain has been included in the path loss of the radar channel.

In the evaluated rural scenario, there exists a dominant line-of-sight (LoS) path marked green and three reflection/scattering paths with much more path loss than the LoS path and marked gray. In this case, the channel behaves like a single-path channel. The transceiver receives the echo from the target vehicle and estimates the distance, relative velocity, and direction of the target vehicle. Since the authors are mainly concerned with the impact of applying CO-PMCW on radar functions like PSLR and radar sensing error, only the echo through the LoS path is included in this work, i.e., the radar detects a single point in the rural scenario.

For the highway scenario, a non-LoS (NLoS) channel is obtained. There also exists a dominant path, however, its dominance is not as strong as the LoS path in the rural scenario.

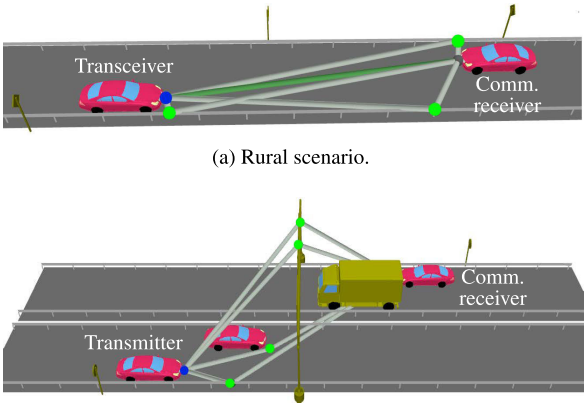

(a) Rural scenario.

(b) Highway scenario.

FIGURE 6. Evaluated rural and highway scenarios in WinProp. The left car acts as a transceiver which transmits the JCAS signal, and the right car performs data reception. In the evaluated rural scenario, there exists a dominant LoS path, and the transceiver also performs radar sensing using the echo. In the highway scenario, a higher influence of multipath fading occurs. [34].

VI. SIMULATION-BASED PERFORMANCE COMPARISON

The following analysis and simulation are based on the introduced system model and channel parameters in section V. In this chapter, the simulation setup and results are described in detail. The comprehensive performance comparison between the PMCW and CO-PMCW systems is implemented.

A. SELF-INTERFERENCE

The interference between the pilot and the data is regarded as a potential side effect of CO-PMCW. Since the two PRNSs have the same period and their time offsets are fixed, the designers can modify their time offsets so that their multiplication is -1 in a period, which extremely suppresses the interference on the data detection and the peak power loss ratio (PPLR) of the radar function.

1) IMPACT ON COMMUNICATIONS FUNCTION

The potential impact of interference exists not only on the data detection but also on the channel estimation. Therefore, the performance of channel estimation and data detection accuracy is analyzed separately in the simulation. Since only the impact of SI is evaluated, the differences in other factors are removed, i.e., in the conducted simulations the PMCW and CO-PMCW systems are configured with the same parameters: the pilot accumulation times of the two systems are the same, i.e., $A = A_c = 10$, the data rate and spreading gain are also equalized, i.e., $G_{PMCW} = G_{CO} = 40.1$ dB. The impact of RF hardware characteristics is ignored, and the average transmission power is normalized to 1 W, i.e., the pilot/data power of the PMCW and CO-PMCW signals is 1 W and 0.5 W, respectively. For simplification, the rural scenario is considered in this section, where the

TABLE 3. Evaluated channel parameters for LoS and NLoS communications and radar with a single point target. The LoS channel model is simulated in the rural scenario, the NLoS channel model is extracted from the highway scenario. The radar channel only considers the LoS path of the communications channel in the rural scenario. [34].

	Paths	Delays τ in ns	Path loss in dB	Phase shift $\Delta\phi$ in $^\circ$	Frequency shift f_D in kHz	RCS in dBsm
Communications LoS	1	67.6	-73.4	-	5.1	-
	2	72.6	-130	21	3.3	-
	3	78.4	-132	205	1.9	-
	4	84.1	-132	101	2.7	-
Communications NLoS	1	74.5	-129	247	4.3	-
	2	79.5	-143.1	350	4.3	-
	3	84.9	-143.2	61.4	3.8	-
	4	93	-143.3	212	3.6	-
Radar	1	135.2	118.44	90	10.2	15

channel behaves like a single-path channel. As a result, the performance of the channel estimation and data detection is only influenced by the SI and SNR.

Different modulation schemes may also lead to different results since a higher modulation scheme brings a higher maximum symbol power $P_{\max}$ and lower minimum symbol power $P_{\min}$, as given in Table 1, where the average power P_{avg} is normalized to 1 W. $P_{\max}$ and $P_{\min}$ are mainly relevant to the impact of interference on channel estimation and data detection, respectively.

- $P_{\max}$: the modulated symbols with the highest power correspond to the highest interference power in the channel estimation process. For Gold codes with a length of 1023, the cross-correlation values can be -1, 63, and -65, the interference can lead to a maximum sidelobe level of e.g., $65 \times 2.82 = 183.3$ with the modulation scheme of 1024-QAM, the corresponding minimum PSLR is $20 \cdot \log_{10}(1023/183.3) = 14.9\,\text{dB}$, which is still high. Thus, a very low (or even negligible) impact on the bit error rate (BER)-SNR curve is expected.
- $P_{\min}$: The symbols with power of $P_{\min}$ is more fragile to interference. For instance, $P_{\min} = 0.0029$ with 1024-QAM. However, the multiplication between PRNS_d and PRNS_p is always -1 in a sequence period, minimizing the interference of the pilot. The pilot suppression ratio is $20 \cdot \log_{10} 1023 = 62\,\text{dB}$, much higher than $P_{\text{avg}}/P_{\min} = 25.4\,\text{dB}$. Therefore, a negligible impact is expected when the data symbol period is one or several times the PRNS period. However, if the data symbol length $G \cdot T_\text{c}$ is below the sequence length $L_\text{c} \cdot T_\text{c}$, the despreading process is no longer a whole-period cross-correlation, a higher impact of modulation schemes occurs.

In the simulation, the channel estimation performance is first analyzed. Because the delay detection and channel transfer function estimation are implemented in different steps, their performance is observed separately. In this work, the delay error rate (DER) is chosen to estimate the delay detection performance as it calculates the probability of incorrect delay detection, i.e.,

$$\text{DER} = \Pr\{\hat{d} \neq d\}, \tag{18}$$

where $\hat{d}$ and d denote the detected delay and true delay, respectively. The normalized mean square error (NMSE) is chosen to measure the accuracy of the channel frequency response (CFR) estimation:

$$\text{NMSE}_H = \frac{\|\hat{H} - H\|^2}{\|H\|^2}, \tag{19}$$

where $\hat{H}$ and H represent the estimated and true channel transfer functions, respectively.

The result of the channel estimation is given in Fig. 7, where the x-axis denotes the SNR, the left and right y-axes show the scales of the DER and NMSE of the channel estimation, whose results are represented by the solid curves and dashed curves, respectively. The results of PMCW (BPSK) and CO-PMCW with modulation schemes of BPSK, QPSK, and 1024-QAM are indicated by the blue rectangular-marked, red circular-marked, yellow asterisk-marked, and purple cross-marked curves. The estimation error of PMCW is chosen as the reference value. Note for PMCW, the pilot symbols and channel estimation accuracy are independent of the data modulation schemes, thus the corresponding DER and NMSE are drawn once in the diagram. The curves corresponding to CO-PMCW are located at approximately 3 dB to the right of the curves of PMCW, corresponding to a 3 dB difference in pilot power (the pilot power of the CO-PMCW-based system is halved due to the simultaneous transmission), i.e., when the pilot power of the two systems is equal, the corresponding channel estimation error values are the same. The result indicates that the impact of SI on channel estimation is negligible. Additionally, the results of the CO-PMCW-based system for modulation schemes from BPSK to 1024-QAM are almost the same, which implies that the modulation schemes have almost no influence on channel estimation. The result follows the analysis explained before.

Besides the channel estimation, the influence of the parallel transmission on the data detection is tested. To this end, BER is chosen as the metric evaluating the communications/data estimation reliability. Assuming the delay, frequency shift, phase offset, and path loss are equalized by a perfect channel estimation or synchronization, the BER is only influenced by the different approaches and modulation schemes. In the simulation, E_b/N_0 is chosen as variable so that the difference between the result curves only comes from the impact of different approaches and modulation schemes.

The result is shown in Fig. 8. The blue, red, yellow, and purple curves denote the result of PMCW and CO-PMCW

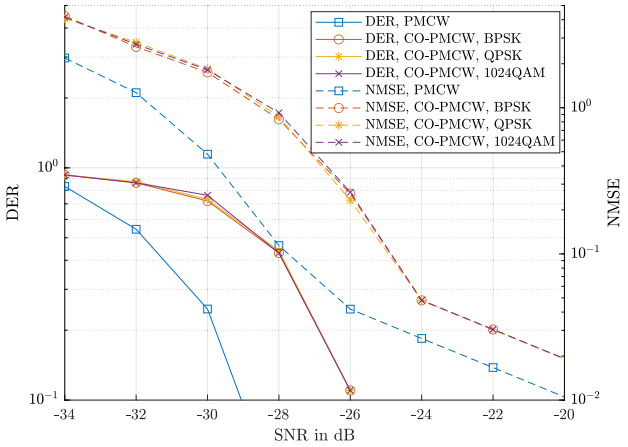

FIGURE 7. Channel estimation accuracy with PMCW and CO-PMCW for different modulation schemes. Since the pilot values and channel estimation process of PMCW are not impacted by the data modulation schemes, the DER, as well as the NMSE of PMCW with different modulation schemes, are constant. Hence, they are drawn once in the figure.

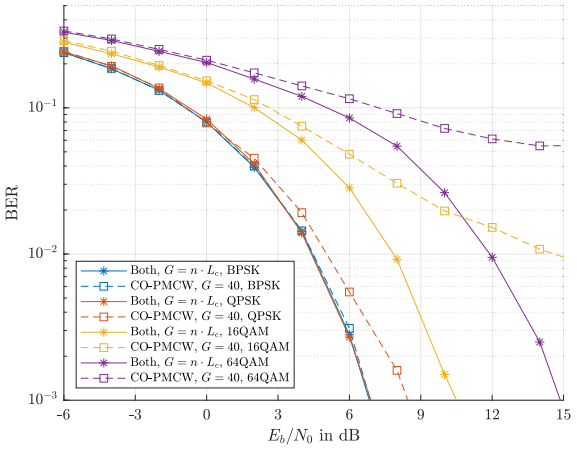

FIGURE 8. BER vs. E_b/N_0 curves with PMCW and CO-PMCW for different modulation schemes. 'Both' denotes the result of both PMCW and CO-PMCW systems. The results of the two systems with the symbol length of integer times the PRNS length are the same, and thus represented by one curve.

with modulation schemes of BPSK, QPSK, 16-QAM, and 64-QAM. The asterisk-marked solid curves represent the BER of CO-PMCW and PMCW whose data length is n times the PRNS length, where n is a positive integer. Note in the case of $G = n \cdot 1023$, the BER of the two PMCW systems with the same modulation scheme are the same, therefore, their results are printed once by the solid curves. The rectangular-marked dashed curves show the BER with CO-PMCW, where the symbol length is shorter than the PRNS length. In this work, $G_{\mathrm{CO}} = 16\,\mathrm{dB}$ is chosen for this case. Following the discussion above, in the cases of $G_{\mathrm{CO}} = n \cdot 1023$, the interference from the pilot sequence has no impact due to the orthogonality between the PRNSs. This orthogonality is broken when the data rate further increases due to the non-optimal CCF when $G_{\mathrm{CO}} < L_{\mathrm{c}}$. The ratio between P_{min} and P_{avg} decreases with higher modulation schemes, thus the data symbols with low power are highly interfered with in this case. As a result, for the CO-PMCW system with $G < L_{\mathrm{c}}$, the impact of SI increases with M.

It is worth noting that the pilot sequence has no interference with data detection when the modulation scheme is BPSK, as the blue asterisk- and rectangular-marked curves are overlapped in Fig. 8. The reason is that the data symbols are the in-phase components, while the pilot symbols are quadrature components, being always orthogonal to the data symbols, as indicated by the constellation diagram in Fig. 2. Other modulation schemes, e.g., QPSK, 8PSK, and M-QAM, suffer from interference since the data symbols have both the in-phase and quadrature components.

It is worth noting that the SNR with the same E_{b}/N_0 and different G is different. If SNR is chosen as the x-axis, the curves corresponding to $G = 16\,\mathrm{dB}$ will be located on the right side of the curves with $G = n \cdot L_{\mathrm{c}}$, and the distance between them is large. In this case, the impact of G and modulation schemes cannot be directly observed in the figure, which is the reason that E_{b}/N_0 is chosen as the x-axis. This setup is also applied in section VI-C.

The estimated influences of SI on communications reliability are summarized here:

- The influence on channel estimation is negligible.
- When the data symbols have length integer times the PRNS length, the impact of SI can be ignored.
- When the data symbols of CO-PMCW signals have a length shorter than the PRNS length, the BER grows with higher modulation schemes ($M \geq 2$).

2) IMPACT ON RADAR FUNCTION

Similar to the process of channel estimation, the parallel transmission also influences the correlation process at the radar receiver. Since the radar only uses the pilot for sensing estimation, it is only necessary to investigate the interference produced by the data sequence. The radar sensing process has a similar feature to channel estimation as both include a correlator bank. As explained in section VI-A1, although the cross-correlation is influenced, the interference power is significantly low compared to the peak value, and its impact on mean absolute error (MAE)-SNR curves is expected to be negligible. However, the increased sidelobe further limits the maximum detectable range, as the echo from targets with longer distances may hide in the sidelobe contributed by the shorter distance components. Therefore, the PSLR and integrated sidelobe ratio (ISLR) of the two systems in the range profile need to be measured, as in this case they directly determine the radar dynamic range. PSLR calculates the power ratio between the peak and the maximum sidelobe, which is desired to be as high as possible. On the contrary, the ISLR is hoped to be sufficiently low, since it corresponds to the ratio between the sum of the sidelobe power and the peak power.

It is worth noting that the pilot power of the CO-PMCW signals is half the PMCW signals, but the radar processing gain $G_{\mathrm{r,PMCW}}$ of PMCW is lower than that of CO-PMCW $G_{\mathrm{r,CO}}$ since the first of each A arrays need to be discarded

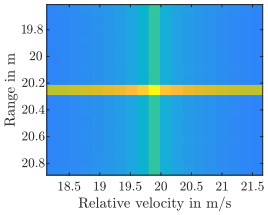

(a) Range-Doppler map of PMCW.

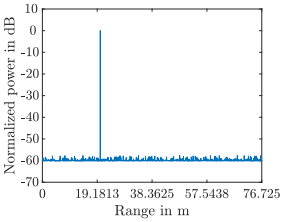

(b) Radar range profile of PMCW.

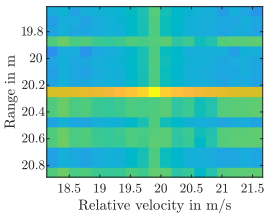

(c) Range-Doppler map of CO-PMCW.

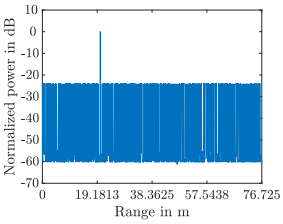

(d) Radar range profile of CO-PMCW.

FIGURE 9. Range-Doppler maps and range profiles of the PMCW- and CO-PMCW-based systems. The noise is not considered in this part. The modulation scheme is BPSK. The bright yellow point corresponding to the target is located at the center of the range-Doppler map. The range profile displays the elements corresponding to the same velocity but different distances, the peak corresponds to the target point. The measured PSLR and ISLR of PMCW are 56.71 dB and −29.72 dB, while the values of CO-PMCW are 23.9 dB and 1.728 dB, respectively.

to avoid the interference from the last transmitted symbol [18], i.e.,

$$G_{\mathrm{r,CO}} = G_{\mathrm{r,PMCW}} + 10 \cdot \log_{10}(\frac{A}{A-1}). \tag{20}$$

When $A = 10$, $G_{\mathrm{r,CO}} = G_{\mathrm{r,PMCW}} + 0.46\,\mathrm{dB}$. Therefore, the radar reliability versus SNR curves of the two systems should have a distance of 2.54 dB in SNR, which will be verified in the simulation. In this work, the MAEs of the estimated range and velocity (denoted by RMAE and VMAE) are observed for this issue, which calculate the main absolute value of the difference between the estimated range and velocity and the realistic values, i.e.,

$$\mathrm{RMAE} = \mathrm{avg}|\hat{r} - r|, \tag{21}$$

$$\mathrm{VMAE} = \mathrm{avg}|\hat{v} - v|, \tag{22}$$

where $\hat{r}$ and $\hat{v}$ correspond to the estimated range and velocity, respectively. The actual range and velocity are represented by r and v.

In the simulation, the range-Doppler map as well as PSLR and ISLR are evaluated first. Fig. 9 shows the range-Doppler map and the range profile of the PMCW and CO-PMCW systems with the modulation scheme of BPSK. The bright yellow point contributed by the detected echo is located at the center of the maps, its corresponding range profile is generated by the sub-orthogonal CCF of the PRNS and interference from the data sequence. The sidelobe power is extremely increased by the CO-PMCW approach. The measured PSLR of PMCW and CO-PMCW is 56.71 dB and 23.9 dB, and their ISLR is −29.72 dB and 1.728 dB, respectively. The increased sidelobe power

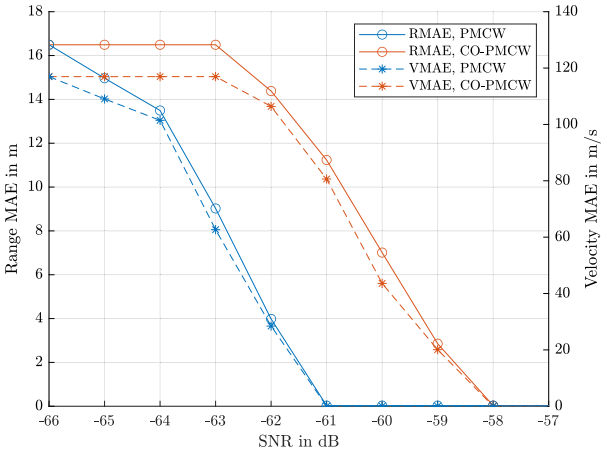

FIGURE 10. MAE versus SNR curves of the PMCW- and CO-PMCW-based systems. The data is BPSK-modulated in the simulation.

further limits the radar sensing range, as other echoes with the same Doppler effect and lower power may not be detected.

The difference in RMAE and VMAE versus SNR curves is given in Fig. 10, where the blue and red curves denote the result of PMCW and CO-PMCW, and the RMAE and VAME are represented by the solid and dotted lines, respectively. The difference in the results between the two approaches is approximately 2.56 dB as expected and comes from the transmission power and radar processing gain. There exists saturation of MAEs when the SNR is sufficiently low and high. In the former case, the estimated range and velocity become randomly distributed values in $[0,\ r_{\mathrm{u}}]$ and $[-v_{\mathrm{u}},\ v_{\mathrm{u}}]$, thus the calculated mean absolute value of error trends to the same value; in the latter case, the MAEs approach 0, with a slight deviation limited in range and velocity resolution.

In conclusion, on the one hand, the halved pilot power makes the receiver slightly more sensitive to noise than the conventional PMCW system. On the other hand, utilizing CO-PMCW leads to interference and thus, a higher sidelobe level at the radar receiver side, which limits the detection range but can be compensated to some extent by methods like increasing L_{c} or changing the type of PRNS.

In case there exist two or more transmitters, Inter-user interference (IUI) also needs to be considered. The IUI also comes from the non-ideal CCF of the spreading codes and thus has a similar impact as the SI. The main difference is that the power of IUI P_{IUI} is variable, whereas the power of SI P_{SI} is constant. Therefore, the impact of IUI is shortly discussed here without further experiment.

We define three scenarios according to the relationship between P_{IUI} and received signal power P_{r}:

- $P_{\mathrm{IUI}} \gg P_{\mathrm{r}}$: in this case, IUI is dominant in interference, thus the SI can be ignored. Since the signal power of the pilot and data is halved by the parallel transmission, the signal-to-interference-plus-noise ratio (SINR) at the receiver in a CO-PMCW system is half the PMCW system, i.e., $SINR_{\mathrm{CO}} \approx \frac{1}{2} SINR_{\mathrm{PMCW}}$.

- $P_{\mathrm{IUI}} \approx P_{\mathrm{r}}$: in this case, the interference power in a CO-PMCW system is approximately 1.5 times that of the PMCW system. Thus, $SINR_{\mathrm{CO}} = \frac{1}{3} SINR_{\mathrm{PMCW}}$.
- $P_{\mathrm{IUI}} \ll P_{\mathrm{r}}$: in this case, SI becomes the dominant interference source. Its impact is the same as discussed in this section.

B. DOPPLER EFFECT AND DYNAMIC ENVIRONMENTS

Maximum Doppler frequency shift $f_{\mathrm{D,max}}$, or Doppler spread f_{DS}, is used to characterize channel time selectivity and dynamic [4]. On the one hand, the communications system designers hope to obtain a slow-fading channel. Whether the channel is fast or slow fading depends not only on channel condition but also on the system configuration like data rate and density of inserted pilot [48]. On the other hand, as reported in [18], [38], and [49], PMCW radar functions like PSLR and PPLR are affected by the Doppler effect, which is a common problem of PMCW-based systems.

1) IMPROVEMENT IN COMMUNICATIONS PERFORMANCE

Improved communication performance in dynamic environments is analyzed as one of the advantages of the CO-PMCW scheme. The data period is desired to be much shorter than the coherence time T_{coh}. If the channel estimation is considered, the time distance between two consecutive inserted pilot symbols should be much shorter than T_{coh}, otherwise, the channel equalization of several data symbols may become unreliable. The corresponding relative speed limitations of PMCW and CO-PMCW are given in (16) and (17), respectively. For a PMCW-based system with a transmission period of $C = 5$, the maximum relative speed should follow $v_{\mathrm{c,max}} \ll 76.17$ m/s. The upper bound of this value is $v_{\mathrm{c,max}} \ll 190.4$ m/s with $C = 2$ and the data rate of 97.8 kbit/s, half of the maximum achievable data rate of PMCW 195.5 kbit/s with $C \to \infty$. For the system with CO-PMCW, $v_{\mathrm{c,max}} \ll 380.9$ m/s in case of $A_{\mathrm{c}} = 10$, which is higher than radar maximum unambiguous velocity. The highest achievable relative speed follows $v_{\mathrm{c,max}} \ll 3809$ m/s when A_{c} equals 1.

In this section, the influence of noise and multi-path fading (coherence bandwidth) are excluded so that the system performance is only affected by channel dynamics (Doppler effect). As for the channel model, to the best of the authors' knowledge, up to now, there has been no result contributing to the LoS small-scale fading process of the 77 GHz V2V channel. The most relevant work is reported in [50], where the 73 GHz vehicle-to-vehicle (V2V) communications channel is measured. The result indicates that the small-scale fading follows the Rician distribution with K-factor of approximately $0 - 4$ dB in short range. The authors of [51] found the mean values of the Rician K-factor for V2V communications in urban, suburban, and rural areas are 1.8 dB, 2.6 dB, and 3 dB, respectively. Therefore, in this section, the authors modeled a Rician fading channel with a K-factor of 3, the parameters like delay, path loss, phase and frequency shifts are the same as the LoS path in Table 3. For simplification, the classical Doppler spectrum, or called Jakes' spectrum, is considered. The channel dynamic is expressed by the relative speed. The highest Doppler shift of the scattering channel corresponds to the scattering components whose direction is opposite to the moving direction of the receiver, while the transmitter and the receiver drive also in an opposite direction, as illustrated in Fig. 6. Thus, the maximum Doppler shift of the scattering components is approximately equal to the Doppler shift of the LoS path.

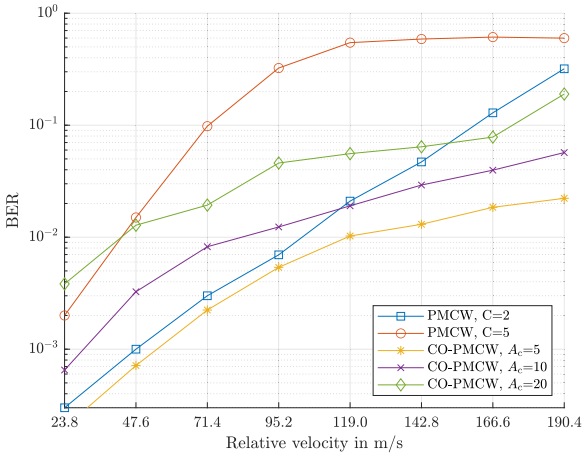

FIGURE 11. BER vs. velocity curves of PMCW with $C = 2$ and 5, and CO-PMCW with $A_{\mathrm{c}} = 5$, 10, and 20.

In the simulation, the relative speed is chosen as the variable and varies from 0 to 190.43 m/s. The Doppler shift of the LoS path and the maximum Doppler shift of the scattering components are the same. The transmission period C of 5 (default in Table 2) and 2 (lowest BER regarding dynamic) are chosen for PMCW. For CO-PMCW, the data rate is default by 50 Mbit/s, and A_{c} is chosen as 5, 10, 20. The result is shown in Fig. 11, where the blue curve denotes the best performance of the PMCW-based system facing dynamic environments as the distance between the pilot symbols is minimized. The BER with $C = 2$ is close to 0.3 with a relative speed of 190.4 m/s. When $C = 5$, as denoted by the red curve, the BER grows rapidly with the relative velocity and approaches 0.3 at the speed of 95.2 m/s. The BER curves with CO-PMCW increase relatively slowly, and lower A_{c} benefits from lower BER. The CO-PMCW approach shows an improved performance in dynamic environments, especially when the channel time selectivity is harsh. On the contrary, the PMCW system shows reliable performance in less dynamic channels, since the interpolator can compensate for the channel parameters in this case. Therefore, when the Doppler effect is low, the PMCW-based system benefits from a relatively reliable interpolation, and the advantage of CO-PMCW becomes not so obvious.

In conclusion: the CO-PMCW scheme performs better in dynamic environments, and this advantage becomes more significant with higher dynamics. The lower the pilot

accumulation time A_c, the better performance against the Doppler effect.

2) RADAR DOPPLER TOLERANCE

From the radar perspective, the researchers are more concerned about the impact of the Doppler effect on the range estimation. The Doppler intolerance is one of the main shortcomings of PMCW. The Doppler effect in the fast time domain leads to a continuously changed phase shift of the chips, degrading the orthogonality of the codes and thus, reduces the peak power and increases the PSLR in the correlation process [52]. Since CO-PMCW utilizes the same radar signal processing scheme as the PMCW systems, the impact of the Doppler effect cannot be compensated.

In the simulation, the impact of the Doppler effect on PPLR, PSLR, and ISLR in the fast time domain (range profile) are measured. The PPLR measures the loss of peak power due to the Doppler effect compared to the peak power with $f_D = 0$ Hz, the PSLR and ISLR reflect the potential sensing error possibility in the fast time domain. The noise is excluded in the simulation so that the measured values only depend on the Doppler effect. Fig. 12 shows the result of PMCW and CO-PMCW, denoted by the blue curve and the red curve, respectively. Note the blue and red curves have extreme differences in values and derivatives, hence they are drawn separately in two subfigures. Fig. 12a shows the PPLR of the two approaches, where the two curves have almost the same degradation ratio with the Doppler effect, implying that the impacts of the Doppler effect on the peak power of the two systems are the same. Fig. 12b and Fig. 12c include the effect on sidelobes. On the one hand, the PSLR and ISLR behaviors of the PMCW-based system are always much better than those of CO-PMCW. On the other hand, the degradation of PSLR and ISLR of CO-PMCW is significantly slower with the growth of the Doppler effect since its sidelobes come not only from the non-ideal ACF but also from interference from the data sequence.

In conclusion, the presented CO-PMCW scheme cannot overcome the Doppler intolerance of the PMCW-based systems. The simultaneous transmission method extremely improves communications function while more or less limiting the radar performance and detectable range, which is regarded as one of the main side effects.

C. COMMUNICATIONS SYSTEM WITH MULTIPATH FADING

Multipath fading is a phenomenon in which the transmitted signal arrives at the receiver antenna from different paths. Delay spread τ_{DS} is an important characteristic of multipath fading as it shows the delay dispersion and is relevant to ISI and frequency selectivity. On the one hand, the data symbol period is desired to be much longer than τ_{DS} to avoid ISI; on the other hand, the data rate should be much lower than channel coherence bandwidth B_{coh} to obtain a flat fading channel. In [53], the authors mentioned that the delay spread of the 77 GHz channel can even reach up to several hundreds of nanoseconds. For instance, a delay spread of 100 ns corresponds to a coherence bandwidth of approximately 10 MHz.

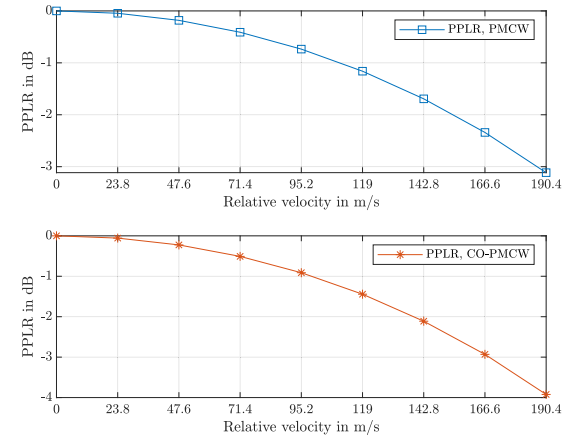

(a) PPLR in range profile.

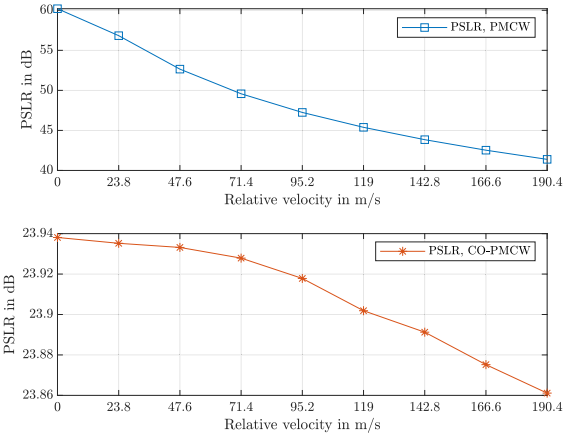

(b) PSLR in range profile.

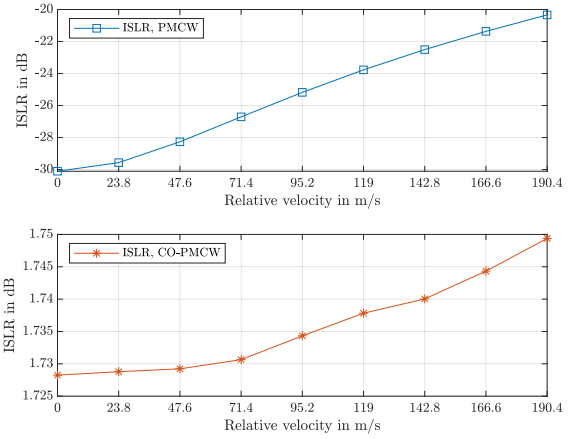

(c) ISLR in range profile.

FIGURE 12. PPLR, PSLR, and ISLR in range profile versus Doppler effect/relative velocity curves of the PMCW- and CO-PMCW-based JCAS systems. The results of the two systems are drawn separately due to their significant difference in values and derivatives.

The PMCW/CDMA-based communications systems usually handle the multipath issues using a Rake receiver which separates the received signals with different delays, in which PRNSs with better ACFs benefit from better suppression of undesired components and thus, less delay spread. For a PMCW system, the despreading process takes one or more PRNS periods, thus the delay spread of the resulting signal is sufficiently suppressed by the whole-period cross-correlation, i.e.,

$$\tau_{\mathrm{DS}} \approx T_{\mathrm{c}} \ll T_{\mathrm{D,PMCW}} = A \cdot L_{\mathrm{c}} \cdot T_{\mathrm{c}}. \tag{23}$$

Besides, the coherence bandwidth is extended to the same order as the signal bandwidth B, while the data bandwidth of PMCW is $B_{\mathrm{D,PMCW}} = \frac{2}{A \cdot L_{\mathrm{c}} \cdot T_{\mathrm{c}}}$, which is 391 kHz in this work, and general much lower than the coherence bandwidth. In consequence, the signal experiences a flat fading.

As discussed in section IV, the communications reliability of CO-PMCW is impacted by the multipath fading in case of high data rate transmission. The channel estimation process is not influenced by the delay spread since the pilot correlator bank takes at least one period of $\mathrm{PRNS_p}$. As for the data rate, on the one hand, when the data symbol period falls below PRNS length, i.e., $G_{\mathrm{CO}} < L_{\mathrm{c}}$, the ACF becomes non-optimal, the suppression of the undesirable signal components is alleviated, increasing the delay spread in the branches of the Rake receiver; on the other hand, the coherence bandwidth is narrowed due to the increased delay spread while the data bandwidth grows, increasing the frequency selectivity. For example, in Table 2, the data rate is 50 Mbit/s, the corresponding spreading gain $G_{\mathrm{CO}} = 40 \ll L_{\mathrm{c}}$, suffering from a weaker suppression of multipath components.

To verify the analyzed impact, a multipath fading channel model is included. The NLoS channel model in Table 3 is used in the simulation. In this section, a wide-sense stationary (WSS)-uncorrelated scattering (US) model is considered, where the channel correlation function is invariant over time, and the paths with different delays or AoA/frequency shifts are uncorrelated [54]. The PMCW communications receiver includes a Rake receiver with MRC to minimize the SNR in the resulting signal. In the simulation, E_{b}/N_0 is chosen as variable, and the BER of the PMCW- and CO-PMCW-based systems with $G = 1$, 40, and $n \cdot L_{\mathrm{c}}$ is observed. The channel dynamic is excluded so that the BER is only influenced by E_{b}/N_0 and multipath fading/delay spread and frequency selectivity. The result is given in Fig. 13, where the blue, red, yellow, and purple curves denote the BER of the PMCW- and CO-PMCW-based systems with $G = 1$, 40, and $n \cdot L_{\mathrm{c}}$, respectively. The result follows the theoretical analysis: when $G = n \cdot L_{\mathrm{c}}$, the undesired delay components are suppressed, thus the BER of PMCW and CO-PMCW are almost the same. When the data period falls below the PRNS length, the orthogonality between the fading components is destroyed, and a higher BER is observed. Note when $G = 40$, the orthogonality is not totally broken, thus the BER is only slightly higher than the orthogonality cases. On the contrary, when $G = 1$, i.e., the data rate is equal to the chip rate,

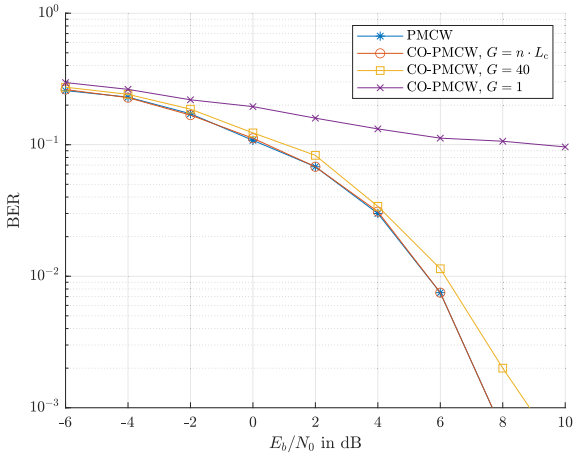

FIGURE 13. BER vs. E_{b}/N_0 curves of PMCW and CO-PMCW with $G = 1$, 40, and $n \cdot L_{\mathrm{c}}$ in multipath fading channel.

where the spreading process does not exist. As a result, the undesired components are not suppressed, hence $T_{\mathrm{D}} \ll \tau_{\mathrm{DS}}$, and $B_{\mathrm{D}} \gg B_{\mathrm{coh}}$, leading to an extremely higher BER.

In conclusion, the data rate of the PMCW system in the multipath fading channel cannot be too high in order to guarantee a reliable transmission. Although the data rate is much improved by the CO-PMCW scheme, due to the limitation of delay spread and coherence bandwidth, the maximum achievable data rate is still significantly lower than OFDM.

VII. CONCLUSION AND OUTLOOK

This work introduces a novel CO-PMCW approach with simultaneously and continuously transmitted pilot and data sequences for future JCAS systems. The two sequences are separated by two orthogonal PRNSs and a phase shift of 90 degrees. The communications receiver utilizes the pilot sequence for channel estimation and then performs equalization and data detection, while the radar receiver only uses the pilot for sensing estimation. On the one hand, the separated transmission process liberates the data rate from the radar function, thus a higher and more flexible data rate is achievable, improving its applicability in future 6G networks. On the other hand, CO-PMCW leads to interference between the pilot and the data sequences, which can more or less impact the radar sensing quality.

Afterward, the advantages and side effects of the CO-PMCW scheme are analyzed theoretically and verified in the simulation. The enhancement in data rate, the improvement of communications performance in dynamic environments, and the side effects like increased PAPR, SI and impact on the multipath fading process are investigated. The pros and cons compared to the conventional PMCW systems are summarized below:

Pros:

- Flexible communications system configuration due to separated pilot and data sequences.
- Higher achievable data rate and spectrum efficiency.

- Better communications behavior in dynamic environments due to continuously transmitted pilot sequence and flexible channel estimator.
- Joint design provides a trade-off between the communications and sensing performance.

Cons:

- The power of the pilot and data are halved due to the parallel transmission.
- Higher PAPR with modulation schemes except for BPSK.
- Higher sidelobe level in radar range profile due to the self-interference.
- More sensitive to IUI.
- Increased hardware complexity and computational effort.

The proposed CO-PMCW scheme has some limitations and unattractive properties, which also exist in the PMCW systems and can be considered as shortcomings compared to other waveforms like OFDM:

- The maximum achievable data rate is limited since when $G < L_c$, the orthogonality in ACF and CCF is destroyed, and the BER is increased by the following factors:
  - -- Interference from the pilot sequence with the modulation schemes except for BPSK.
  - -- Multipath fading.
  - -- Interference from other users.

  Therefore, the achievable data rate of the improved PMCW system is lower than OFDM.
- The Doppler intolerance of PMCW is still not solved.

Compared to the radar-centric design waveforms, the CO-PMCW approach has a much better communications performance with slightly degraded radar properties. On the contrary, compared to the communications-based waveforms like OFDM, the CO-PMCW scheme has a relatively lower data rate but less PAPR and better radar functions like maximum unambiguous range and velocity due to the good property of PMCW radar [18]. It is worth noting that there exists an option to configure the power ratio between the pilot and data sequences for better adaptation to different environments and requirements. For instance, when the radar needs to detect objects at longer distances, the data power could be reduced and thus, the radar PSLR in the range profile is increased. It is also feasible to only transmit the pilot sequence or CDMA-like communications signal if only the radar or communications function is necessary, resulting in a trade-off between these two functions. Therefore, we consider the presented CO-PMCW scheme to belong to the category of joint design instead of the radar-centric design.

As the parallel transmission leads to interference between the pilot and data sequences, it is essential to include methods like increasing L_c or finding other spreading sequences with better ACF and CCF properties to suppress the impact of the interference. There already exist studies focusing on this topic. For instance, in [38], the authors compared the CCF of the Gold codes, almost perfect auto-correlation sequences (APASs), and zero correlation zone (ZCZ) sequences. It was shown that Gold codes have a relatively better CCF, while there exists a special zone in the CCF of ZCZ sequences where the values are zero. Applying the ZCZ sequences can avoid SI, but the maximum range is further limited in the special zone. In [55], the authors introduced a novel orthogonal minimum correlation spreading code with a significantly improved performance in ACF and CCF. Comparing the correlation properties of different spreading codes in the CO-PMCW JCAS system is left for future research.

From the application perspective, the performance of the JCAS systems is quite different in realistic scenarios. The SINR is increased by the SI, halved pilot and data power, and the increased PAPR, limiting the maximum transmission range. The SI issues can be compensated by optimizing the PRNSs, while the other two problems are difficult to solve. As a result, CO-PMCW is currently considered to be a perfect candidate for short-range JCAS systems. Verifying this assumption, or evaluating the maximum sensing and communication range of CO-PMCW, is left for future works.

AUTHOR CONTRIBUTION

Methodology and system design, Yanpeng Su; simulation setup, measurements, Yanpeng Su, and Victor Shatov; supervision, Maximilian Lübke, and Norman Franchi; writing-original draft, Yanpeng Su; writing-review and editing, all authors.

REFERENCES

[1] V. Petrov, G. Fodor, J. Kokkoniemi, D. Moltchanov, J. Lehtomaki, S. Andreev, Y. Koucheryavy, M. Juntti, and M. Valkama, "On unified vehicular communications and radar sensing in millimeter-wave and low terahertz bands," *IEEE Wireless Commun.*, vol. 26, no. 3, pp. 146–153, Jun. 2019.

[2] K. Ramasubramanian and K. Ramaiah, "Moving from legacy 24 GHz to state-of-the-art 77-GHz radar," *ATZelektronik Worldwide*, vol. 13, no. 3, pp. 46–49, Jun. 2018.

[3] J. Hasch, E. Topak, R. Schnabel, T. Zwick, R. Weigel, and C. Waldschmidt, "Millimeter-wave technology for automotive radar sensors in the 77 GHz frequency band," *IEEE Trans. Microw. Theory Techn.*, vol. 60, no. 3, pp. 845–860, Mar. 2012.

[4] R. He, C. Schneider, B. Ai, G. Wang, Z. Zhong, D. A. Dupleich, R. S. Thomae, M. Boban, J. Luo, and Y. Zhang, "Propagation channels of 5G millimeter-wave vehicle-to-vehicle communications: Recent advances and future challenges," *IEEE Veh. Technol. Mag.*, vol. 15, no. 1, pp. 16–26, Mar. 2020.

[5] J. Choi, V. Va, N. Gonzalez-Prelcic, R. Daniels, C. R. Bhat, and R. W. Heath Jr., "Millimeter-wave vehicular communication to support massive automotive sensing," *IEEE Commun. Mag.*, vol. 54, no. 12, pp. 160–167, Dec. 2016.

[6] P. K. Singh, S. K. Nandi, and S. Nandi, "A tutorial survey on vehicular communication state of the art, and future research directions," *Veh. Commun.*, vol. 18, Aug. 2019, Art. no. 100164.

[7] F. Arena and G. Pau, "An overview of vehicular communications," *Future Internet*, vol. 11, no. 2, p. 27, Jan. 2019. [Online]. Available: https://www.mdpi.com/1999-5903/11/2/27

[8] J. Nidamanuri, C. Nibhanupudi, R. Assfalg, and H. Venkataraman, "A progressive review: Emerging technologies for ADAS driven solutions," *IEEE Trans. Intell. Vehicles*, vol. 7, no. 2, pp. 326–341, Jun. 2022.

[9] J. A. Zhang, Y. J. Guo, and K. Wu, *Introduction to Joint Communications and Sensing (JCAS)*. Hoboken, NJ, USA: Wiley, 2023, pp. 1–30.

[10] T. Wild, V. Braun, and H. Viswanathan, "Joint design of communication and sensing for beyond 5G and 6G systems," *IEEE Access*, vol. 9, pp. 30845–30857, 2021.

[11] F. Liu, Y. Cui, C. Masouros, J. Xu, T. X. Han, Y. C. Eldar, and S. Buzzi, "Integrated sensing and communications: Toward dual-functional wireless networks for 6G and beyond," *IEEE J. Sel. Areas Commun.*, vol. 40, no. 6, pp. 1728–1767, Jun. 2022.

[12] M. Chafii, L. Bariah, S. Muhaidat, and M. Debbah, "Twelve scientific challenges for 6G: Rethinking the foundations of communications theory," *IEEE Commun. Surveys Tuts.*, vol. 25, no. 2, pp. 868–904, Jul. 2023.

[13] M. Hoffmann et al., "A secure and resilient 6G architecture vision of the German flagship project 6G-ANNA," *IEEE Access*, vol. 11, pp. 102643–102660, 2023.

[14] M. A. Uusitalo, P. Rugeland, M. R. Boldi, E. C. Strinati, P. Demestichas, M. Ericson, G. P. Fettweis, M. C. Filippou, A. Gati, M.-H. Hamon, M. Hoffmann, M. Latva-Aho, A. Pärssinen, B. Richerzhagen, H. Schotten, T. Svensson, G. Wikström, H. Wymeersch, V. Ziegler, and Y. Zou, "6G vision, value, use cases and technologies from European 6G flagship project Hexa-X," *IEEE Access*, vol. 9, pp. 160004–160020, 2021.

[15] J. A. Zhang, F. Liu, C. Masouros, R. W. Heath Jr., Z. Feng, L. Zheng, and A. Petropulu, "An overview of signal processing techniques for joint communication and radar sensing," *IEEE J. Sel. Topics Signal Process.*, vol. 15, no. 6, pp. 1295–1315, Nov. 2021.

[16] J. A. Zhang, M. L. Rahman, K. Wu, X. Huang, Y. J. Guo, S. Chen, and J. Yuan, "Enabling joint communication and radar sensing in mobile networks—A survey," *IEEE Commun. Surveys Tuts.*, vol. 24, no. 1, pp. 306–345, 1st Quart., 2022.

[17] M. Goppelt, H.-L. Blöcher, and W. Menzel, "Analytical investigation of mutual interference between automotive FMCW radar sensors," in *Proc. German Microw. Conf.*, Mar. 2011, pp. 1–4.

[18] L. Giroto de Oliveira, B. Nuss, M. B. Alabd, A. Diewald, M. Pauli, and T. Zwick, "Joint radar-communication systems: Modulation schemes and system design," *IEEE Trans. Microw. Theory Techn.*, vol. 70, no. 3, pp. 1521–1551, Mar. 2022.

[19] F. Engels, P. Heidenreich, M. Wintermantel, L. Stäcker, M. A. Kadi, and A. M. Zoubir, "Automotive radar signal processing: Research directions and practical challenges," *IEEE J. Sel. Topics Signal Process.*, vol. 15, no. 4, pp. 865–878, Jun. 2021.

[20] D. Ma, N. Shlezinger, T. Huang, Y. Liu, and Y. C. Eldar, "Joint radar-communication strategies for autonomous vehicles: Combining two key automotive technologies," *IEEE Signal Process. Mag.*, vol. 37, no. 4, pp. 85–97, Jul. 2020.

[21] G. Hakobyan and B. Yang, "High-performance automotive radar: A review of signal processing algorithms and modulation schemes," *IEEE Signal Process. Mag.*, vol. 36, no. 5, pp. 32–44, Sep. 2019.

[22] J. Rong, F. Liu, and Y. Miao, "Integrated radar and communications waveform design based on multi-symbol OFDM," *Remote Sens.*, vol. 14, no. 19, p. 4705, Sep. 2022. [Online]. Available: https://www.mdpi.com/2072-4292/14/19/4705

[23] K. M. Braun, "OFDM radar algorithms in mobile communication networks," Ph.D. dissertation, Karlsruher Institut für Technologie (KIT), Karlsruhe, Germany, 2014.

[24] M. Lübke, J. Fuchs, V. Shatov, A. Dubey, R. Weigel, and F. Lurz, "Simulation environment of a communication system using CDMA at 77 GHz," in *Proc. Int. Wireless Commun. Mobile Comput. (IWCMC)*, Jun. 2020, pp. 1946–1951.

[25] A. Bourdoux, U. Ahmad, D. Guermandi, S. Brebels, A. Dewilde, and W. Van Thillo, "PMCW waveform and MIMO technique for a 79 GHz CMOS automotive radar," in *Proc. IEEE Radar Conf. (RadarConf)*, May 2016, pp. 1–5.

[26] Y. Su, V. Shatov, M. Lübke, and N. Franchi, "Improving resource efficiency of PMCW-based JCRS systems: Simultaneous transmission of pilot and data via orthogonal codes," in *Proc. IEEE 34th Annu. Int. Symp. Pers., Indoor Mobile Radio Commun. (PIMRC)*, Sep. 2023, pp. 1–7.

[27] Z. Ni, J. A. Zhang, X. Huang, K. Yang, and F. Gao, "Parameter estimation and signal optimization for joint communication and radar sensing," in *Proc. IEEE Int. Conf. Commun. Workshops (ICC Workshops)*, Jun. 2020, pp. 1–6.

[28] F. Liu, C. Masouros, A. P. Petropulu, H. Griffiths, and L. Hanzo, "Joint radar and communication design: Applications, state-of-the-art, and the road ahead," *IEEE Trans. Commun.*, vol. 68, no. 6, pp. 3834–3862, Jun. 2020.

[29] V. Giannini, D. Guermandi, Q. Shi, A. Medra, W. Van Thillo, A. Bourdoux, and P. Wambacq, "A 79 GHz phase-modulated 4 GHz-BW CW radar transmitter in 28 nm CMOS," *IEEE J. Solid-State Circuits*, vol. 49, no. 12, pp. 2925–2937, Dec. 2014.

[30] D. Guermandi, Q. Shi, A. Dewilde, V. Derudder, U. Ahmad, A. Spagnolo, I. Ocket, A. Bourdoux, P. Wambacq, J. Craninckx, and W. Van Thillo, "A 79-GHz 2 × 2 MIMO PMCW Radar SoC in 28-nm CMOS," *IEEE J. Solid-State Circuits*, vol. 52, no. 10, pp. 2613–2626, Jul. 2017.

[31] S. H. Dokhanchi, M. R. B. Shankar, Y. A. Nijsure, T. Stifter, S. Sedighi, and B. Ottersten, "Joint automotive radar-communications waveform design," in *Proc. IEEE 28th Annu. Int. Symp. Pers., Indoor, Mobile Radio Commun. (PIMRC)*, Oct. 2017, pp. 1–7.

[32] M. Lübke, J. Fuchs, V. Shatov, A. Dubey, R. Weigel, and F. Lurz, "Combining radar and communication at 77 GHz using a CDMA technique," in *IEEE MTT-S Int. Microw. Symp. Dig.*, Nov. 2020, pp. 1–4.

[33] V. Ziegler, P. Schneider, H. Viswanathan, M. Montag, S. Kanugovi, and A. Rezaki, "Security and trust in the 6G era," *IEEE Access*, vol. 9, pp. 142314–142327, 2021.

[34] M. Lübke, Y. Su, A. J. Cherian, J. Fuchs, A. Dubey, R. Weigel, and N. Franchi, "Full physical layer simulation tool to design future 77 GHz JCRS-applications," *IEEE Access*, vol. 10, pp. 47437–47460, 2022.

[35] A. L. T. Chinchilla, "Synchronization and channel estimation in OFDM: Algorithms for efficient implementation of WLAN systems," Ph.D. dissertation, Brandenburgischen Technischen Universität, 2004.

[36] S. Colieri, M. Ergen, and A. Puri, "A study of channel estimation in OFDM systems," in *Proc. IEEE 56th Veh. Technol. Conf.*, Sep. 2002, pp. 894–898.

[37] S. P. Jadhav and V. S. Hendre, "Performance of maximum ratio combining (MRC) MIMO systems for Rayleigh fading channel," *Int. J. Sci. Res. Publications*, vol. 3, no. 2, pp. 1–4, 2013.

[38] J. Overdevest, F. Jansen, F. Uysal, and A. Yarovoy, "Doppler influence on waveform orthogonality in 79 GHz MIMO phase-coded automotive radar," *IEEE Trans. Veh. Technol.*, vol. 69, no. 1, pp. 16–25, Jan. 2020.

[39] Z. Xinyu, "Analysis of M-sequence and gold-sequence in CDMA system," in *Proc. IEEE 3rd Int. Conf. Commun. Softw. Netw.*, May 2011, pp. 466–468.

[40] F. Bozorgi, P. Sen, A. N. Barreto, and G. Fettweis, "RF front-end challenges for joint communication and radar sensing," in *Proc. 1st IEEE Int. Online Symp. Joint Commun. Sens.*, Feb. 2021, pp. 1–6.

[41] M. Lübke, Y. Su, and N. Franchi, "Evaluating RF hardware characteristics for automotive JCRS systems based on PMCW-CDMA at 77 GHz," *IEEE Access*, vol. 11, pp. 28565–28584, 2023.

[42] A. Behravan, R. Baldemair, S. Parkvall, E. Dahlman, V. Yajnanarayana, H. Björkegren, and D. Shrestha, "Introducing sensing into future wireless communication systems," in *Proc. 2nd IEEE Int. Symp. Joint Commun. Sens.*, Mar. 2022, pp. 1–5.

[43] A. Goldsmith, *Wireless Communication*. Cambridge, U.K.: Cambridge Univ. Press, 2005.

[44] A. Zajic, *Mobile-to-Mobile Wireless Channels*. London, U.K.: Artech House, 2012.

[45] F. Hlawatsch and G. Matz, *Wireless Communications Over Rapidly Time-Varying Channels*, 1st ed. New York, NY, USA: Academic, 2011.

[46] C. F. Mecklenbrauker, A. F. Molisch, J. Karedal, F. Tufvesson, A. Paier, L. Bernado, T. Zemen, O. Klemp, and N. Czink, "Vehicular channel characterization and its implications for wireless system design and performance," *Proc. IEEE*, vol. 99, no. 7, pp. 1189–1212, Jul. 2011.

[47] N. Shaik and P. K. Malik, "A comprehensive survey 5G wireless communication systems: Open issues, research challenges, channel estimation, multi carrier modulation and 5G applications," *Multimedia Tools Appl.*, vol. 80, no. 19, pp. 28789–28827, Aug. 2021.

[48] D. Tse and P. Viswanath, *Fundamentals of Wireless Communication*. Cambridge, U.K.: Cambridge Univ. Press, 2005.

[49] C. Sturm and W. Wiesbeck, "Waveform design and signal processing aspects for fusion of wireless communications and radar sensing," *Proc. IEEE*, vol. 99, no. 7, pp. 1236–1259, Jul. 2011.

[50] H. Wang, X. Yin, X. Cai, H. Wang, Z. Yu, and J. Lee, "Fading characterization of 73 GHz millimeter-wave V2V channel based on real measurements," in *Communication Technologies for Vehicles*. Cham, Switzerland: Springer, 2018, pp. 159–168.

[51] S. Zhu, Tahereh. S. Ghazaany, S. M. R. Jones, R. A. Abd-Alhameed, J. M. Noras, T. Van Buren, J. Wilson, T. Suggett, and S. Marker, "Probability distribution of Rician K-factor in urban, suburban and rural areas using real-world captured data," *IEEE Trans. Antennas Propag.*, vol. 62, no. 7, pp. 3835–3839, Jul. 2014.

[52] S. Xu and A. Yarovoy, "Doppler shifts mitigation for PMCW signals," in *Proc. Int. Radar Conf. (RADAR)*, Sep. 2019, pp. 1–5.
[53] M. Lübke, J. Fuchs, A. Dubey, M. Frank, N. Franchi, and F. Lurz, "Antenna setup for future joint radar-communications—Characteristics and mounting positions," *Adv. Radio Sci.*, vol. 20, pp. 55–65, Mar. 2023.
[54] M. Pätzold, *Mobile Radio Channels*. Hoboken, NJ, USA: Wiley, 2011.
[55] S. Pradhan, S. Chattopadhyay, and S. Raut, "A novel orthogonal minimum correlation spreading code in CDMA system," *Int. J. Wireless Microw. Technol.*, vol. 4, no. 2, pp. 38–52, Mar. 2014.

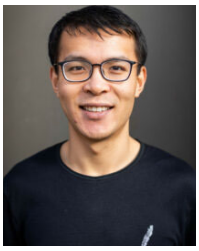

YANPENG SU (Member, IEEE) received the B.Sc. degree in electrical engineering and automation from China University of Petroleum (East China) (UPC), Qingdao, China, in 2018, and the M.Sc. degree in electrical engineering from Friedrich-Alexander-Universität Erlangen-Nürnberg (FAU), Erlangen, Germany, in 2022. In 2022, he joined the Chair of Electrical Smart City Systems, FAU, as a Research Assistant. His current research interests include channel modeling and waveform design for joint communications and radar sensing and coordinated multipoint radar sensing system design.

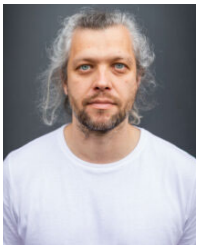

VICTOR SHATOV (Member, IEEE) received the M.Sc. degree in communications and multimedia engineering (CME) from the University of Erlangen-Nuremberg (FAU), in 2021. He was a Student Research Assistant with the Chair of Electronics Engineering (LTE) during his studies. He wrote his master's thesis with the German Aerospace Center (DLR), Communication and Navigation Department. In February 2022, he joined the Chair of Electrical Smart City Systems (ESCS) as a Research Assistant. His research interests include joint communication and sensing, radar technology, emitter localization, signal classification, and distributed real-time spectrum sensing.

NORMAN FRANCHI (Member, IEEE) received the Dipl.-Ing. (M.S.E.E.) and Dr.-Ing. (Ph.D.E.E.) degrees in electrical, electronic and communications engineering (EEI), in 2007 and 2015, respectively. He is currently a Full Professor (W3) with Friedrich-Alexander-Universität Erlangen-Nürnberg (FAU), Germany, where he heads the Chair of Electrical Smart City Systems. From 2007 to 2011, he worked in the automotive research and development sector as a System and Application Engineer for advanced networked control system design. From 2012 to 2015, he was a Research Associate with the Institute for Electronics Engineering, FAU, focused on software-defined radio-based V2X communications. From 2015 to 2021, he was with Gerhard Fettweis' Vodafone Chair with Dresden University of Technology (TU Dresden), where he was the Senior Research Group Leader of resilient mobile communications systems and 5G industrial campus networks. From 2019 to 2020, he was the Managing Director of the 5G Laboratory GmbH, Germany. In 2020, he founded the company Advancing Individual Networks (AIN) GmbH, Germany, a technology start-up for design, optimization, and operation of IIoT networks. He is a member of the IEEE ISAC initiative, Open 6G Hub Germany, 5G Laboratory Germany, and 6G Platform Germany. Furthermore, he is also an Advisory Board Member of the Industrial Radio Laboratory Germany (IRLG) and the KI Park Deutschland. His research interests include 6G, joint communications and sensing, resilient and secure systems, the IIoT, open RAN, V2X, and green ICT for smart cities.

MAXIMILIAN LÜBKE (Member, IEEE) received the B.S. degree in medical engineering and the M.S. degree in electrical engineering from Friedrich-Alexander-Universität Erlangen-Nürnberg, Erlangen, Germany, in 2017 and 2018, respectively, and the Dr.-Ing. (Ph.D.E.E.) degree, in 2023. In 2019, he joined the Institute for Electronics Engineering, FAU, as a Research Assistant. In 2022, he switched to the Chair of Electrical Smart City Systems. He is currently heading the group of radio technology and networks with the Chair of Electrical Smart City Systems. His current research interests include joint radar and communications systems and circuit design with respect to automotive applications. He was a recipient of the Best Paper Award of the ACM International Conference on Nanoscale Computing and Communication, in 2019, and of the EAI International Conference on Bio-Inspired Information and Communications Technologies, in 2020, respectively.